3D imaging of undissected optically cleared *Anopheles stephensi* mosquitoes infected with *Plasmodium* parasites

Mariana De Niz[1*], Jessica Kehrer[2], Nicolas M.B. Brancucci[3#], Federica Moalli[4Δ], Emmanuel G. Reynaud[6], Jens V. Stein[5], Friedrich Frischknecht[2]

[1] Institute of Cell Biology, Heussler Research Group, University of Bern, Bern, Switzerland

[2] Center for Infectious Diseases, Integrative Parasitology, Heidelberg University Medical School, Im Neuenheimer Feld 344, 69120 Heidelberg, Germany

[3] Wellcome Centre for Integrative Parasitology, Institute of Infection, Immunity & Inflammation, University of Glasgow, Glasgow, UK

[4]Theodor Kocher Institute, University of Bern, Bern, Switzerland

[5] Department of Oncology, Microbiology and Immunology, University of Fribourg, Fribourg, Switzerland

[6] School of Biomolecular and Biomedical Science, University College Dublin, Ireland

[*] Current address: Instituto de Medicina Molecular João Lobo Antunes, Faculty of Medicine, University of Lisbon, Portugal

[#] Current address: Swiss Tropical and Public Health Institute, University of Basel, Basel, Switzerland

[Δ] Current address: San Raffaele Scientific Institute, Milan, Italy

Corresponding author: Mariana De Niz mariana.deniz@medicina.ulisboa.pt

Keywords

Mosquitoes; Parasitology; Infection biology; Optical projection tomography; Light sheet fluorescence microscopy; Vectors.

Summary statement

Various diseases are transmitted by mosquitoes but their imaging is hindered by heavy light scattering. We present here 3D reconstructions of *Plasmodium*-infected, optically cleared mosquitoes, imaged using optical projection tomography and light sheet fluorescence microscopy.

Abstract

Malaria is a life-threatening disease, caused by Apicomplexan parasites of the *Plasmodium* genus. The *Anopheles* mosquito is necessary for the sexual replication of these parasites and for their transmission to vertebrate hosts, including humans. Imaging of the parasite within the insect vector has been attempted using multiple microscopy methods, most of which are hampered by the presence of the light scattering opaque cuticle of the mosquito. So far, imaging of the *Plasmodium* mosquito stages depended on either sectioning or surgical dissection of important anatomical sites, such as the midgut and the salivary glands. Optical projection tomography (OPT) and light sheet fluorescence microscopy (LSFM) enable imaging fields of view in the centimeter scale whilst providing micrometer resolution. In this paper, we present reconstructions of the whole body of *Plasmodium*-infected, optically cleared *Anopheles stephensi* mosquitoes and their midguts. The 3D-reconstructions from OPT imaging show detailed features of the mosquito anatomy and enable overall localization of parasites in midguts. Additionally, LSFM imaging of mosquito midguts shows detailed distribution of oocysts in extracted midguts.

Introduction

Arthropod-borne diseases constitute an enormous public health burden world-wide. Some of the most medically relevant diseases in tropical areas caused by mosquitoes include malaria, dengue, yellow fever, Chikungunya fever, Zika fever, encephalitis, and filariasis (Beaty and Marquardt, 1996; Eldridge and Edman, 2000; Kettle, 1995; Lehane, 1991). The blood-sucking behavior of female mosquitoes is necessary for egg development and constitutes the link to vertebrate hosts, as pathogens are transmitted during mosquito blood meals. There are approximately 3,500 species of mosquitoes grouped into two main sub-families and 41 genera (CDC, 2014). The two subfamilies are the *Anophelinae* and the *Culicinae*, which not only display important anatomical and physiological differences, but vary in their clinical significance as disease vectors of the pathogens they transmit. Recent outbreaks of Zika and dengue fever, as well as the constant pressure of malaria on many regions of the developing world continue to demand a better understanding of host-pathogen interactions in the vector. Advances in this field are likely to inform researchers across various disciplines about improved ways of blocking pathogen transmission. In this paper we explore 3D imaging of intact (in contrast to dissected), optically cleared *Anopheles* mosquitoes as vectors for the *Plasmodium* parasite, the causing agent of malaria. We envisage that the technique is equally useful to *Aedes* and *Culex* mosquitoes, both of which are important vectors of a wide range of pathogens.

Malaria causes over 200 million infections and over 400,000 human deaths per year (WHO, 2016). Although hundreds of vertebrate-infecting *Plasmodium* species exist, only five species are infectious to humans. During their life cycle, *Plasmodium* parasites adopt various forms, both invasive and replicative, within the vertebrate host and the mosquito vector (reviewed by (Aly et al., 2009; Silvie et al., 2008)). While rodent-infecting parasites have been imaged in all relevant tissues within mice (skin, liver, blood and bone marrow) (De Niz et al., 2019a,b,c,d; De Niz et al., 2020), imaging of parasites within the living mosquito has remained elusive and limited to the passive floating of sporozoites in the hemolymph and proboscis (Frischknecht et al., 2004, 2006). The development of sporozoites *in vivo* in the midgut and their entry into mosquito salivary glands remains to be visualized.

As an optically opaque cuticle surrounds these organs, most of the imaging achieved so far has relied on dissection of these organs and imaging *in situ*.

The possibility to visualize biological tissue in 3D has proven to be invaluable for understanding complex processes in various tissue forms – including that of insects. For centuries, imaging at depth required the physical sectioning of tissue due to photon scattering. The imaging limit of conventional microscopy in terms of penetration depth is set by a physical parameter of photons known as the mean free path (MFP) (reviewed by Ntziachristos, 2010) which refers to the collision events of these wave-particles. With widefield epifluorescence microscopy, high quality imaging is possible when the thickness of tissue sections is within 10-50 µm (**Figure 1A**). With confocal and multi-photon microscopy, greater penetration depths (>500 µm) can be achieved (**Figure 1B**); however, this penetration depth is still impractical for highly resolved 3D digital reconstructions of large specimens.

Novel 3D imaging techniques such as optical projection tomography (OPT) (Sharpe et al, 2002) and light sheet fluorescence microscopy (LSFM) also known as selective plane illumination microscopy (SPIM) or ultramicroscopy, allow visualization of large objects without the need of physical sectioning (Huisken et al, 2004) (see commentary by Reynaud et al 2015). A pre-requisite for these imaging techniques applied to opaque samples is optical clearance, as in transparent media light propagates deeper into tissues, (reviewed by (Ntziachristos, 2010). In order to generate a transparent sample, tissues can be chemically cleared using various solvents and imaging techniques (reviewed by (De Niz et al., 2019a)).

After rendering the specimen transparent, OPT imaging is achieved via tissue trans- and epi-illumination over multiple projections (Sharpe et al., 2002) as the specimen is rotated through 360 degrees in angular steps around a single axis **(Figure 1C)**. Virtual sections are reconstructed from the acquired images using a back-projection algorithm (Kak and Slaney 1988). OPT achieves penetration depths of up to 15 millimeters (Sharpe et al., 2002), and allows high resolution 3D image reconstructions of the sample's complete volume.

Conversely, LSFM uses a thin plane of light (or light sheet), shaped by a cylindrical lens or a laser scanner to exclusively illuminate the focal plane of the sample (**Figure 1D**) (Huisken et al., 2004)

and is characterized by high imaging speed, reduced toxicity, and reduced photobleaching (reviewed by Pampaloni et al., 2007). 3D image formation is based on raw images being assembled after translation or rotation of the entire sample. The difference between OPT and LSFM in terms of mesoscopic imaging is that OPT images are isotropic (without distortion in any 3D axis), but the focal depth is deliberately large and low numerical aperture (NA) objectives are used yielding low resolution. Conversely, LSFM images are anisotropic (with higher resolution in the x and y axes than in *z*), but usually work with higher NA objectives and therefore achieve a high resolution, up to single cell level. OPT can also be designed for single cell resolution but at the expense of sample size imaging capacity (reviewed in (Liu et al 2019)).

Open source, custom built-versions and free software for LSFM (OpenSPIM) (Gualda et al., 2013; Pitrone et al., 2013) and OPT (OptiJ) (Vallejo Ramirez et al., 2019) have been generated, making these imaging platforms easily accessible across laboratories and disciplines. OPT and/or LSFM have been used to image various specimens (reviewed in (De Niz et al., 2019a)) including a detailed reconstruction of the anatomy of the flight musculature of a *Drosophila* fly, its nervous and digestive systems, and ß-galactoside activity throughout the fly's whole body (Jährling et al., 2010; McGurk et al., 2007). Using OPT or LSFM, fluorescence reporters and antibody labeling can be used to reveal specific structures or protein localizations. Recent work showed the development of *P. berghei* (*Plasmodium* parasites infecting mice) at fixed points in optically cleared mosquitoes using CUBIC (Clear Unobstructed Brain/Body Imaging Cocktails and Computational Analysis) (Mori et al., 2019). Here, we generated 3D reconstructions of optically cleared *Anopheles stephensi* mosquitoes infected with mCherry- or GFP-expressing *Plasmodium berghei* parasites using OPT and LSFM. We present a comparative evaluation of different clearance protocols and discuss their value concerning different applications and research questions. Ultimately, following testing of the various protocols, we performed further work with the method we found most efficient for clearance while preserving mCherry fluorescence. Thus, the reconstructions we present are based on mosquitoes rendered transparent using Murray's clear (Dent et al., 1989; Dodt et al., 2007). Our approach provided detailed views of the anatomy of the mosquito head, thorax and abdomen. We envisage that the presented techniques will be of use for the study of pathogen and vector biology.

Figure 1

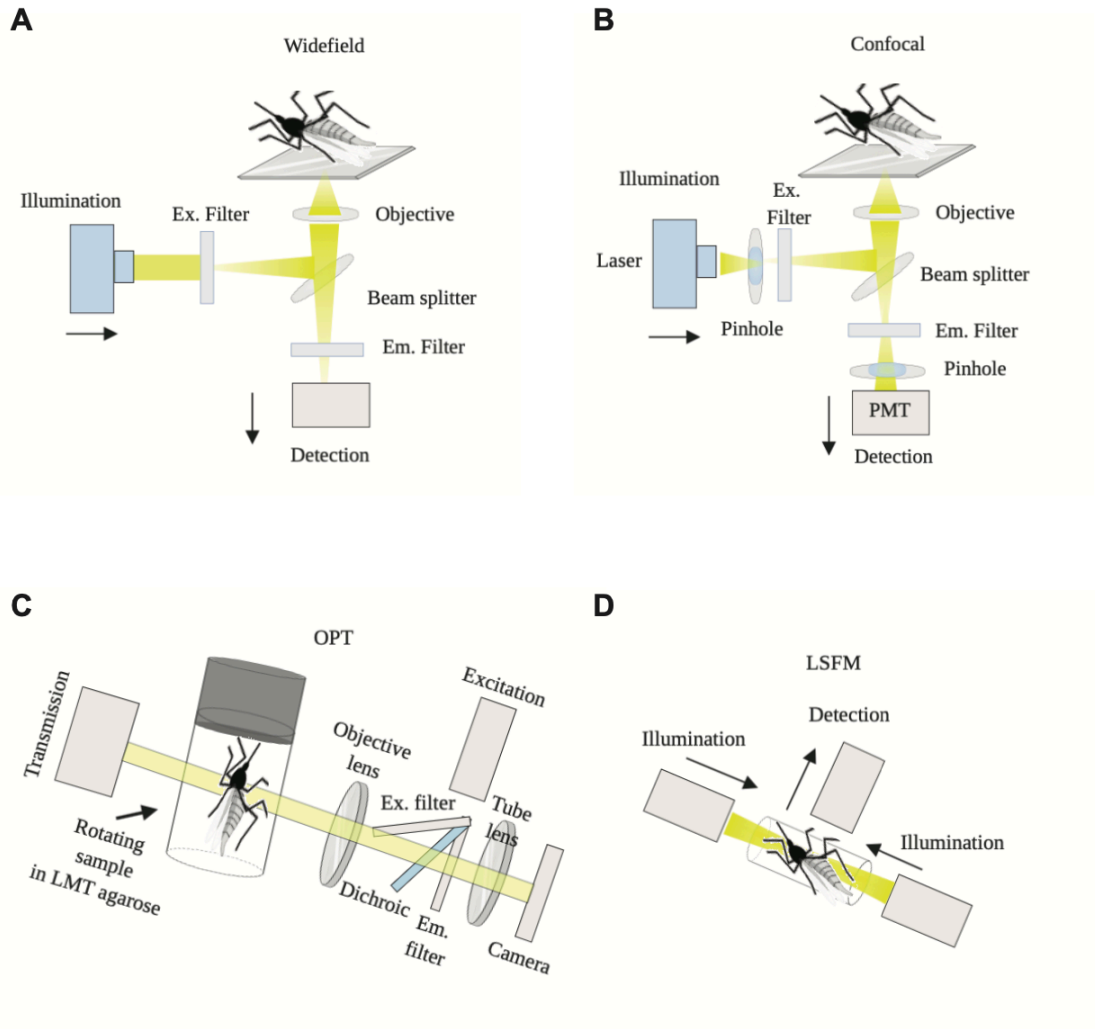

Figure 1. Microscopy methods used for imaging mosquitoes. A) 'Inverted' widefield microscopy: White light is filtered to the appropriate emission wavelength, and the emitted fluorescent light is projected onto a camera. **B)** Confocal microscopy: laser light is focused onto the specimen and a pinhole excludes out of focus light. Instead of a camera, photomultiplier tubes (PMTs) collect photons. **C)** Optical projection tomography: The optically cleared specimen is embedded in agarose, attached to a metallic cylinder within a rotating stage, and suspended in an index-matching liquid to reduce scattering and heterogeneities of refractive index throughout the specimen. Images are captured at distinct positions as the specimen is rotated. The axis of rotation is perpendicular to the optical axis, so that straight line projections going through the sample can be generated, and collected on the camera. **D)** Light sheet fluorescence microscopy: The sample is embedded in agarose, and suspended within a sample holder inside an index-matching liquid. A thin (µm range) slice of the sample is illuminated perpendicularly to the direction of observation. Scanning is performed using a plane of light, which allows very fast image acquisition.

Results

Optical clearance of infected and uninfected *Anopheles stephensi* mosquitoes.

A major hurdle for whole-body mosquito imaging is light scattering due to presence of the cuticle. To overcome this hurdle, we used optical clearing methods to increase light depth penetration and reduce scattering. While multiple clearance techniques have been developed over the past decade, we tested four different techniques based on either organic solvents or water, and we compared them in terms of a) time to achieve mosquito transparency (**Figure 2A**), b) preservation of fluorescent dyes in full mosquitoes (**Figure 2B** and **Figure 2C**) and excised midguts (**Figure 2D**) as well as c) conservation of mosquito tissue morphology (**Figure 2E**). These methods are BABB (Murray's clear) (Dent et al.,1989; Dodt et al., 2007), Sca*l*eS (Hama et al., 2015), SeeDB (Ke et al., 2013), and 3DISCO (Ertürk et al., 2012). Results are summarized in table 1and **Figure 2**.

Mosquito clearance and transparency was successful using 3DISCO and BABB.

First, we compared tissue transparency achieved by 3DISCO, BABB, Sca*l*eS and SeeDB. Optical clearance was defined to be successful (100% transparency) as soon as imaging of the entire width of the mosquito body with OPT and confocal microscopy was possible. The two solvent-based protocols, BABB and 3DISCO, achieved clearance of the mosquito cuticle within a median time of 6.5 days (SD = 4.46; n=50 in triplicate experiments) and 21 days (SD = 8.6; n=50 in triplicate experiments) respectively (**Figure 2A**). Conversely to BABB and 3DISCO, the sorbitol-based clearance method Sca*l*eS achieved only up to 80% transparency in all mosquitoes tested, within a median time of 32.5 days (SD = 6.02, n=50 in triplicate experiments). Next, we tested SeeDB, a protocol that combines use of the water-soluble clearing agents fructose and urea. Similar to what we found for Sca*l*eS, clearance of the cuticle was only partial after 34.5 days of incubation (SD = 7.9, n = 50 in triplicate experiments) using these water-based methods (**Figure 2A**).

Figure 2

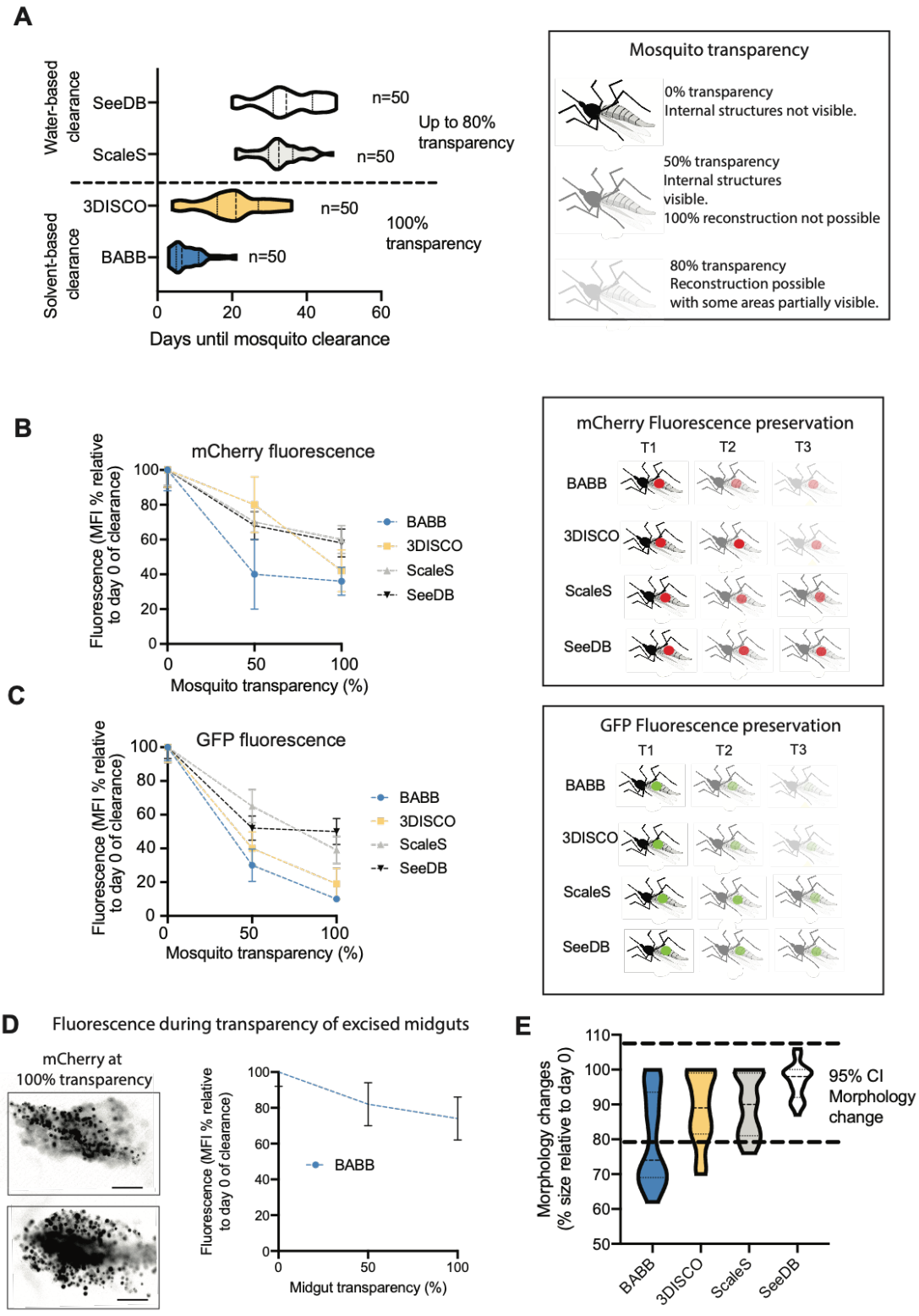

Figure 2. Quantitative and semi-quantitative assessment of tissue clearance methods as applied to *A. stephensi* mosquitoes. A) Determination of time of clearance for achievement of transparency of *Anopheles* mosquitoes. For each method, 50 mosquitoes were embedded in ultrapure low melting temperature agarose gel,

and processed as required for SeeDB, Sca*l*eS, 3DISCO and BABB clearance. Mosquitoes were imaged by confocal microscopy, and 100% transparency determined as the possibility to image through the full sample at a high level of detail and without significant light scattering. Two-way ANOVA test between methods for days required for mosquito clearance, p = 0.06. **B)** mCherry fluorescence intensity and **C)** GFP fluorescence intensity were measured in all infected mosquitoes at the time of euthanasia (at day 12 post-infection) prior to clearance, and this value was defined as 100% for each sample. Fluorescence was measured again at various times of clearance. Graph B shows the average fluorescence percentage relative to time 0, at time points whereby 50% and maximum transparency were achieved. Dots represent average percentage. Error bars represent standard deviations. ANOVA tests resulted in p-values of 0.86 and 0.82 for B and C respectively. **D)** Mosquito midguts were excised and optically cleared using BABB. mCherry fluorescence intensity was then measured throughout midgut clearance. Images show fluorescence by the time the midgut was fully cleared. Results shown in the graph are the mean and standard deviations of 20 midguts measured. Scale bar: 20 µm. **E)** Semi-quantitative representation of morphological changes in mosquitoes following incubation in BABB, 3DISCO, SeeDB or Sca*l*eS. Mosquito sizes were measured at point 0 (day of euthanasia), and measured again at the time of maximum transparency. Dotted lines represent the range considered not significant, based on all measures regardless of method used. Only BABB resulted in tissue shrinkage leading to a median size decrease of 26% (SD = 13). Sample size for each method was n = 50 mosquitoes. Two-way ANOVA test between all clearance methods for morphology, p = 0.12.

Fluorescence preservation significantly differs among clearance methods and fluorophores used.

In a next step, we compared the preservation of parasite-expressed fluorophores (mCherry or GFP) in the mosquito midgut by monitoring the emitted fluorescence until >80% clearance was reached with 3DISCO, BABB, Sca*l*eS and SeeDB (**Figure 2B**). Our findings for 3DISCO showed that the cuticle is fully cleared within a median time of 21 days. However, compared to untreated mosquitoes, mCherry signal was reduced by 20% (SD = 16.2) by the time the mosquitoes were 50% cleared, and by 58% (SD = 13) by the time mosquitoes were 100% cleared. BABB achieved fastest optical clearance, yet fluorescence decreased by 60% (SD = 20.2) at 50% mosquito transparency, and by 64% (SD =12.0) when mosquitoes were fully transparent. Sca*l*eS and SeeDB were slowest to achieve optical clearance, yet fluorescence preservation with both methods was significantly higher than with either BABB or 3DISCO. With Sca*l*eS clearance, fluorescence decreased by 30% (SD = 6.5) at 50% mosquito transparency, and by 40% (SD = 8.0) by the time mosquitoes were fully transparent. With Sca*l*eS,

fluorescence decreased by 32% (SD = 8.2) at 50% mosquito transparency, and by 42% (SD = 8.5) by the time mosquitoes were fully transparent (**Figure 2B**).

In cleared mosquitoes harbouring GFP-expressing parasites, the loss of fluorescence was significantly higher compared to mCherry, both at 50% and 100% optical mosquito clearance. Particularly, both solvent-based methods (i.e. BABB and 3DISCO) resulted in 70-80% fluorescence loss by the time full clearance was achieved (**Figure 2B and 2C**). To determine specific fluorescence loss, we measured fluorescence intensity throughout clearance time in excised mosquito midguts. The time for achieving transparency in midguts was half of that needed to achieve transparency of full mosquitos, and fluorescence intensity was better preserved, as shown in **Figure 2D**. Data shown are the result of measuring 20 midguts at day 8-10 post-feed.

Different clearance methods conserve mosquito morphology equally well

Clearance methods can introduce morphology artefacts, including dehydration or expansion of biological samples. To determine the morphological alterations introduced by each of the methods tested, we measured relative size change of the samples by the time of maximum optical clearance. We found that 3DISCO, SeeDB Sca*l*eS and BABB induced slight morphological changes in the samples, with the median size being 89% (SD = 10), 90% (SD = 8.5), 98% (SD = 5.0), and 77% (SD = 13) the size of the same samples prior to clearance, respectively (range of significance is shown between dotted lines, **Figure 2E**).

Considering all parameters, we chose the method with the greatest tissue clearance success within a short time-frame, and therefore we decided to use BABB as the method of choice for all subsequent experiments reported in this work. Our rationale for this choice is that in subsequent work we will aim at method optimization for fluorescence preservation, however we considered that tissue transparency was a significant advantage for various relevant anatomical observations without the need of fluorophores, and BABB was the most efficient method to achieve this.

OPT enables visualization of the entire anatomy of intact adult mosquitoes

Cleared adult *Anopheles stephensi* mosquitoes were three-dimensionally reconstructed from OPT projections (**Figure 3A-B; Movie 1**), to represent various features of the head, the thorax, and the lower body including the midgut *in situ*. Following clearance, the absorption, reflection and auto-fluorescence of the cuticle were reduced to an extent that internal organs of the mosquito could be visualized (**Figure 3**).

The mosquito head is specialized for processing sensory information, and feeding. The mosquito has compound eyes made up of multiple lenses called ommatidia, which could be faithfully reconstructed by OPT (**Figure 3C, top panels**). Olfaction is an additional primary sensory modality of mosquitoes. OPT enabled imaging of the antennae, the mandibles and maxillae lining the alimentary canal, and the maxillary palps (**Figure 3C, top panels**). OPT also allowed detailed visualization of the proboscis and its structures (all structures mentioned above are marked with arrowheads).

The *Anopheles* mosquito thorax is specialized for locomotion, and is divided into three segments, the prothorax, the mesothorax, and the metathorax, all of which were readily distinguished by OPT (**Figure 3B**; note that the surface rendered image has been previously shown in (De Niz et al., 2019a)). Each thoracic segment supports a pair of legs (3 pairs in total), while the mesothorax additionally bears a pair of wings (**Figure 3C, bottom panels)**. Moreover, the thorax harbors the dorsal blood vessel, the tracheal and dorsal tubes (or heart), the foregut, and various nerve ducts (**Figure 3A-3B**).

Finally, the abdomen (**Figure 3A-3B**) is specialized for food digestion, reproduction, and egg development. The *Anopheles* mosquito abdomen is long and can be divided into up to 10 segments, clearly visible by OPT (**Figure 3B, right panel**). Unlike the thorax, segments I to VIII can expand significantly upon ingestion of a blood meal. This expansion was clearly visible in fed mosquitoes. Segment VIII bears the terminal anus of male and female mosquitoes. In females, segments IX and X bear the gonopore, and a post-genital plate, while in males, segments IX and X harbour a pair of clawed claspers and an aedigus. All structures of the thorax, abdomen and reproductive segments were readily visualized by OPT (**Figure 3A** and **Figure 3B**) and are marked by arrows respectively.

Figure 3

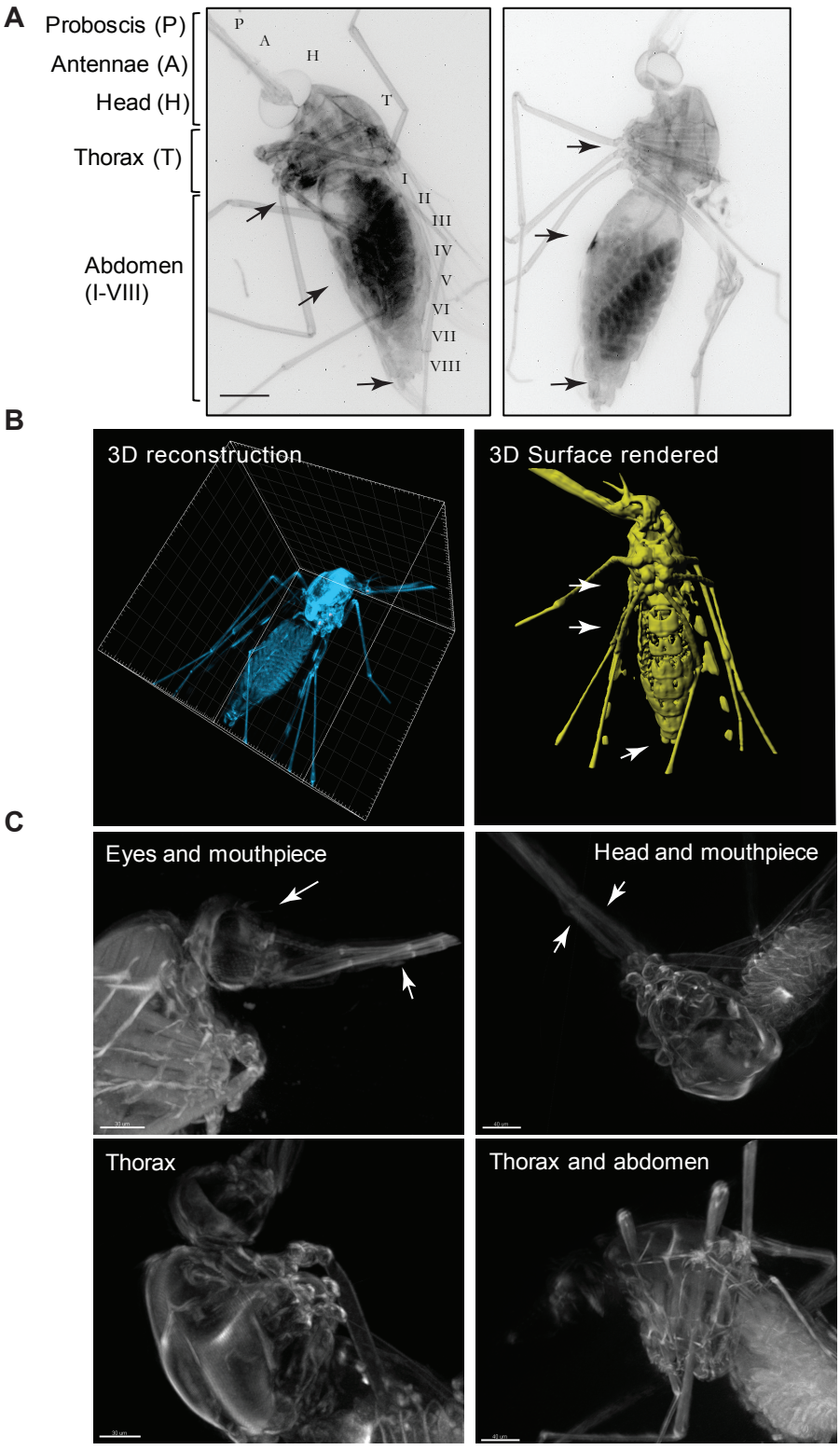

Figure 3. Visualization of an optically cleared *Anopheles stephensi* female mosquito. A) 2D reconstruction of two reconstructed mosquitoes showing detailed views of the head structures (H) including the antennae (A), and the proboscis (P) and the eyes. Detailed view of the thorax is also possible, as well as of all segments of the

abdomen. Scale bar: 500 µm. **B)** 3D reconstruction and clear view of all body cavities of an optically cleared mosquito (left panel). 3D reconstruction and rendering of the mosquito (right panel) clearly showing abdominal segments, thorax and head features (previously shown in (De Niz et al., 2019a)); see movie S1. **C)** Close-up views of various views of the optically cleared mosquito body including the eyes and mouthpieces (side view, upper left panel), the head and mouthpiece (top view, upper right panel), the thorax (side view, lower left panel), and the abdomen including eggs (side view, lower right panel). Scale bar: 200 µm.

OPT enables imaging *Plasmodium* parasites within the isolated midguts and salivary glands

We used mCherry- or GFP-tagged *P. berghei* to observe parasite distribution within entire mosquitoes at various times post blood-feed, however, encountered significant autofluorescence arising from the eggs. We imaged isolated mosquito midguts by LSFM (**Figure 4**) and an OPT time course experiment using intact mosquitoes.

Immediately after a blood-feed on an infected mouse, no fluorescent signal from parasites was detected, yet the mosquito anatomy could be visualized at high level of detail. At day 16 post-infection, we detected strong mCherry signals in the salivary glands, the mesothorax, the base of the wings, and the midgut (**Figure 4A**). However, the signal was diffuse and did not allow for detection of individual sporozoites or oocysts in the complete mosquito. Also detailed insights into multiple mosquitoes imaged shows strong signal arising from autofluorescence which in some cases is indistinguishable from mCherry-specific fluorescence and in some cases is not (**Figures S2 and S3)**. In contrast, LSFM performed on isolated midguts clearly shows individual *P. berghei* oocysts across a full rotation of the sample (**Figure 4B and Movie 2**). In excised cleared midguts, our technique allowed for the first time, full quantification of oocyst numbers throughout parasite development. Moreover, in optically cleared mosquitoes, egg quantification in the undissected mosquitoes, was also possible. To our knowledge, this is the first work allowing quantitative analysis of this type.

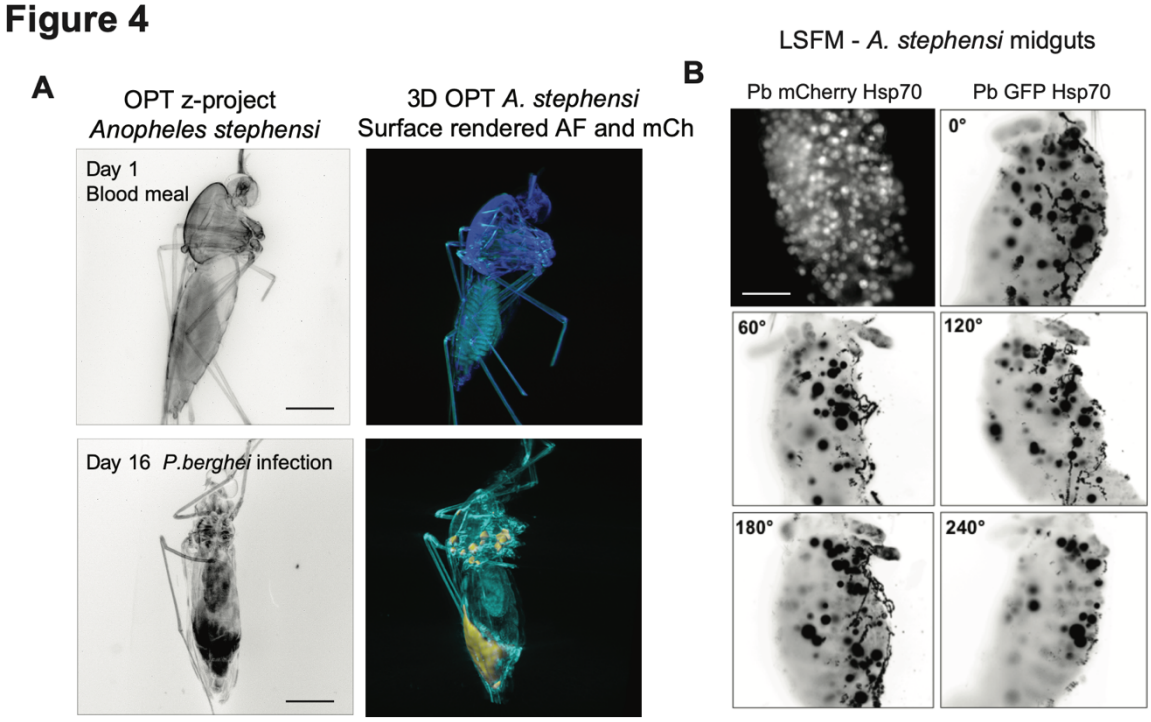

Figure 4. Visualization of *Plasmodium*-infected *Anopheles stephensi* female mosquitoes. (A) 3D project (B&W) and 3D reconstructions of mosquitoes at the beginning and end of *P. berghei* infection as well as egg development (yellow rendering). Scale bar 500 µm. **(B)** Isolated *P. berghei*-infected mosquito midguts imaged by LSFM. Oocysts are shown in white (*P. berghei*-mCherry) or black (*P. berghei*-GFP). Scale bars: 100 µm.

Discussion

One of the major hurdles for whole-body mosquito imaging is light scattering due to presence of the cuticle. Optical clearing techniques enable an increase of light depth penetration and generally reduce light scattering by replacing cellular water with solutions that have a refractive index similar to that of the cell membrane. Lipids in cell membranes are dominant scattering agents in biological tissues, and optical clearing methods can obtain approximately uniform refractive index profiles by removing them. Reduced light scattering ultimately leads to higher spatial resolution and greater contrast. Various clearance techniques have been developed, and have proven to be advantageous for imaging different tissues of interest. These techniques include the use of organic solvents (Abe et al., 2016; Becker et al., 2012; Dodt et al., 2007; Ertürk et al., 2012), water ((Hama et al., 2015, 2011; Ke et al., 2013), and

electrophoresis-based protocols (Chung et al., 2013; Poguzhelskaya et al., 2014). In this work, four techniques were tested for mosquito clearance, and were compared in terms of a) time to achieve tissue transparency, b) preservation of fluorescence signal in mosquitoes infected with mCherry-expressing *Plasmodium berghei* parasites (albeit not effective preservation of GFP signal) and c) resulting mosquito tissue morphology following treatment.

Clearing with BABB achieved the fastest clearance (+/- 6 days) of the mosquito cuticle but led to slight shrinkage of the tissue due to dehydration. Unexpectedly, BABB enabled preservation of mCherry fluorescence signal during extended time periods. However, when mosquitoes were infected with GFP-expressing *P. berghei* parasites, fluorescence was rapidly lost, suggesting that different fluorescent proteins react differently to this clearance method, as previous work has also suggested (Abe et al., 2016). 3DISCO allowed cuticle clearance only after a median time of 21 days. Fluorescence signal from the midguts, as assessed using an epifluorescence microscope, was lost at similar rates as in mosquitoes cleared using BABB. Equally, mCherry and GFP fluorescence decreased at different rates, with GFP fluorescence being lost faster. We then investigated mosquito clearance with Sca*l*eS, a sorbitol-based clearance protocol renowned for its successful preservation of tissue morphology and fluorescence signal (Hama et al., 2015). Although we noticed that the morphology and fluorescence were indeed optimally preserved in treated mosquitoes, clearance was only partial after 30 days of sample incubation, showing that although the method could be successfully applied for use in brains and samples of similar composition, it was suboptimal for clearance of the mosquito cuticle. Finally, SeeDB has been reported to achieve fast clearing results of brain tissue with optimal preservation of tissue integrity and fluorescence signal (Ke et al., 2013). As for Sca*l*eS, although mosquito tissue preservation and fluorescence signal were optimally preserved with SeeDB, full tissue clearance was not possible even after 30 days of incubation.

Altogether, we conclude that the use of BABB was most useful for our purposes. This method allowed full clearance of the mosquito and visualizing overall distribution of parasites throughout the infection, albeit without sufficient detail to distinguish individual parasites using OPT. Compared to GFP, we found mCherry to be more stable in BABB cleared mosquitoes. However, we are confident

that further optimization will also yield satisfactory results for the Sca*l*eS, SeeDB, and 3DISCO techniques.

We imaged the mosquito head using OPT, which allowed observing the eyes, salivary glands, and proboscis in great detail. While techniques such as scanning electron microscopy and synchrotron X-ray tomography have provided important findings on the anatomy of the mosquito head, both require complex equipment and sample preparation. OPT requires relatively simple sample preparation and, in contrast to the aforementioned techniques, is also compatible with the use of fluorescent probes and dyes. We envisage that imaging of intact optically cleared mosquitoes using the absorption mode of OPT (i.e. using ß-galactosidase-dependent blue staining) will enable tracking of pathogen-induced changes in gene expression (Sharpe et al., 2002), and changes in expression of specific components in the mosquito's sensory systems.

We know that changes in insect sensory responses and behavior are likely to increase the chances of parasite transmission, and are thought to arise either from changes in the expression of salivary gland components (Choumet et al., 2007; Ribeiro et al., 1984; Rossignol et al., 1984), or from the modulation of the mosquito nervous system. These changes may be induced by parasites, including *Plasmodium* (Lefevre et al., 2007). While mosquito imaging has largely focused on the sites of parasite replication and residence i.e., the midgut and salivary glands, respectively, imaging of specific molecules and gene expression levels in other tissues that potentially influences behaviour has not yet been performed but could be achievable with OPT or LSFM. Our work was successful in the clearance of the mosquito thorax and visualization of internal structures. Further study of these structures in undissected mosquitoes might shed light into the mosquito's biology and vectorial capacity.

Internally, the abdomen harbors the ovaries and oviduct in females, the hind-gut, the Malpighian tubules, and the midgut (or stomach). The latter is essential for replication of pathogens, including *Plasmodium* and various viruses including West Nile, Chikungunya, and dengue. Labeling the midgut as well as other anatomical structures with specific antibodies, or cell type-specific fluorescent reporters in both mosquitoes and pathogens would be a valuable tool for studying host-pathogen interactions at a whole-body level. OPT allowed visualization of diverse parasite localizations within infected mosquitoes. However, we could not improve on the resolution obtained from uncleared

mosquitoes infected with GFP-expressing parasites. Hence higher resolution OPT and LSFM, or OPTiSPIM, would be relevant to study parasites *in vivo*.

In conclusion, we have shown that adult *Anopheles* mosquitoes can be cleared efficiently, and that this allows for transmission of white and fluorescent light to detect anatomical features of parasite-infected mosquitoes in 3D using OPT and LSFM. The results presented here will hopefully fuel the development of whole-body imaging technologies to allow for the discovery of important host-pathogen interactions in the malaria field.

Materials and Methods

Ethics statement

Mouse infections were carried out under the approval of the Animal Research Ethics Committee of the Canton Bern, Switzerland (Permit Number: 91/11 and 81/11); the University of Bern Animal Care and Use Committee, Switzerland; and the German Tierschutzgesetz (Animal Rights Laws). We have followed the Ethical Guidelines for the Use of Animals in Research. For all mosquito feeds, female mice 5–8 weeks of age, weighing 20-30 g at the time of infection were used. Mice were purchased from Harlan or Charles River laboratories. Blood feeding to mosquitoes was performed under ketavet/dorbene anaesthesia, and all efforts were made to minimize animal suffering.

Parasites lines and their maintenance in mosquitoes

P. berghei-ANKA lines were used in this study to infect mice used for mosquito feeds. *P. berghei*-mCherry$_{Hsp70}$ (Burda et al., 2015), *P. berghei*-GFP$_{Hsp70}$ and PbmCherry$_{Hsp70}$FLuc$_{ef1\alpha}$ (Prado et al., 2015) express fluorescent mCherry that localizes to the cytosol of the parasite, and is expressed constitutively throughout the parasites' life cycle.

Balb/c mice were treated with phenylhydrazine two days prior to intra-peritoneal (i.p.) infection with *P. berghei*-mCherry$_{Hsp70}$ or PbmCherry$_{Hsp70}$FLuc$_{ef1\alpha}$. After 3 days of infection, gametocyte exflagellation was assessed. Upon confirming exflagellation, the infected mice were used to feed various cages with 100–150 *Anopheles stephensi* female mosquitoes. Mice were anaesthetized with a

combination of Ketasol/Dorbene anaesthesia, and euthanized with CO_2 after completion of the feed. Afterwards, mosquitoes were fed until use, with 8 % fructose containing 0.2 % PABA.

Mosquito embedding

Adult female *Anopheles stephensi* mosquitoes were killed at various times following feeds on mice infected with *P. berghei,* and fixed overnight at 4°C in a 1:1 mixture of 4% paraformaldehyde in 1x PBS and 100% ethanol. Mosquitoes were then washed 3 times in 1xPBS for 5 minutes each time. Washed mosquitoes were embedded in 1.3% ultrapure low-melting agarose (Invitrogen) in deionized water. Gels containing the mosquitoes were transferred for at least 2h to 4°C. Using a single-edge blade, the gel was then trimmed into a block containing a single mosquito in the centre.

BABB (Murray's clear)-based mosquito dehydration and clearance

Agarose blocks containing the mosquitoes at all times post blood-feed (including 2 h, 20 h, and day 1 through day 16), were dehydrated in a graded ethanol series (50, 70, 90, 96, and 100%) for 1 h each. Mosquitoes were then transferred to another flask containing 100% ethanol, and dehydrated overnight. Finally, mosquitoes were incubated in a clearing solution consisting of two parts benzyl benzoate and one part benzyl alcohol (BABB, also known as Murray's clear) (Dodt et al., 2007; Genina et al., 2010; Gerger et al., 2005) for at least 10 days, until they became transparent.

3DISCO-based mosquito dehydration and clearance

Previous work showed that tetrahydrofluoran (THF) in combination with dibenzyl ether (DBE), fully clears multiple mouse tissues including the lymph nodes, spinal cord, lungs, spleen and brain, while successfully preserving fluorescent signals (Becker et al., 2012; Ertürk et al., 2012). Two clearing protocols were adapted for use in mosquitoes, namely a relatively short protocol consisting of dehydration in a graded THF series (50, 70, 80 and 100%) for 30 minutes each, followed by 2 further 30 minute incubations in 100% THF. This was followed by a 20-minute incubation in dichloromethane (DCM), and a 15-minute incubation in DBE. The long protocol consisted on dehydration in the graded

THF series for 12 h each, followed by 2x 12 h incubations in 100% THF. This was followed by clearance in DBE, without the intermediate DCM step.

SeeDB-based mosquito dehydration and clearance

In 2013, Ke and colleagues (Ke et al., 2013) first published a water-based optical clearing agent called SeeDB, which had the advantage of preserving fluorescence, including that of lipophilic tracers, while also preserving sample volume and cellular morphology. In order to prepare fructose solutions, D(-)-fructose was dissolved in distilled H_2O at 65°C, and upon cooling to 25°C, α-thioglycerol was added to give a final concentration of 0.5%. Mosquitoes were initially fixed in 4% PFA, and embedded into 1% ultrapure agarose in dH_2O. Fixed mosquitoes were then serially incubated in 20%, 40% and 60% fructose, each for 4 h, followed by a 12 h incubation in 80% fructose, a 12 h incubation in 100% fructose, and incubation in SeeDB at either 37°C or 50°C.

Microscopy – Optical projection tomography (OPT)

OPT scanning was performed according to the manufacturer's instructions (Bioptonics). Filter sets were exciter 425/40, emitter LP475 for autofluorescent signal, exciter 480/20, emitter LP515 for green fluorescent signal; and exciter 545/30, emitter 617/75 for red fluorescent signal. Raw data were converted into 3D voxel datasets using NRecon software from Bioptonics. Reconstructed virtual *xyz* data sets were exported as .tif files and analyzed with IMARIS (Bitplane) for visualization and/or isosurface reconstruction of parasite distribution in the mosquitoes. IMARIS reconstructions were carefully adjusted to fit original NRecon reconstructions.

Light Sheet Fluorescence Microscopy (LSFM)

Light sheet fluorescence microscopy scanning was performed using a commercially available Ultramicroscope system (LaVision BioTec). Light was produced by a 200-mW laser that illuminates the sample from both sides by two co-localized thin sheets of light to compensate for absorption gradients within the tissue. A 10x objective with a NA of 0.3 was used.

Microscopy - Confocal imaging

Confocal imaging of dissected midguts and salivary glands for validation of the observations performed by OPT and LSFM was performed using a Leica SP8-STED microscope. Midguts and salivary glands were imaged using a 20x air objective, using a white light laser at a wavelength of 550nm, and a 63x oil immersion objective using a white laser at wavelengths 405 and 488 nm. The LASX software was used for image acquisition.

Sample mounting for OPT and LSFM

Microscope setups for conventional widefield and confocal systems are remarkably different to those of OPT and LSFM (**Figure 1**). For conventional fluorescence microscopy samples are usually placed on glass bottom dishes or microscope slides in which they are overlaid with a coverslip. Preparation for OPT and LSFM requires placing the sample in a medium- or liquid-filled chamber that enables rotation or motion during image acquisition (**Figure S1A**). In order to take full advantage of the 3D imaging technique all the specimens need to be mounted into a special metal sample holder that is inserted into the chamber from a magnet above (**Figure S1B**). The specimen may be embedded in a gel such as low melting agarose dissolved in the medium or buffer of choice (**Figure S1C**). The medium keeps the sample in place without influencing the penetration of light and imaging quality.

Author contributions

MDN and JK performed mosquito infections and mosquito clearance. MDN and FM imaged mosquitoes by OPT. MDN, JK and EGS imaged mosquitoes by LSFM. MDN and JK reconstructed images. NMBB generated diagrams. EGS, JVS and FF coordinated experiments. MDN and FF wrote the manuscript with input by all coauthors.

Acknowledgements

We are grateful to Volker Heussler (IZB, University of Bern) for his intellectual input and funding of this project. We thank Uroš Kržič for acquisition and processing of Movie 2 included in this manuscript. We thank Renzo Danuser (Theodor Kocher Institute, University of Bern) for important input for the

OPT technique, and Leandro Lemgruber (Wellcome Trust Centre for Molecular Parasitology) for his input on image processing. OPT and confocal microscopy was performed on equipment supported by the Microscopy Imaging Center, University of Bern, Switzerland. We thank Ernst Stelzer and Pavel Tomancak for motivation to use SPIM.

Declaration of conflicts of interest

On behalf of all co-authors, the corresponding author states that there is no conflict of interest.

Funding

This work was supported by the European Union's Seventh Framework Programme (FP7/2007-2013) under grant agreement 242095: EVIMalar (Prof. Volker Heussler and MDN), by a Swiss National Foundation Grant (310030_159519 to Prof. Volker Heussler) and an ERC starting grant (StG 281719) and the Chica and Heinz Schaller Foundation (FF).

Bibliography

Abe, J., Ozga, A.J., Swoger, J., Sharpe, J., Ripoll, J., Stein, J. V., 2016. Light sheet fluorescence microscopy for in situ cell interaction analysis in mouse lymph nodes. *J Immunol Methods.* 431, 1–10. doi:http://dx.doi.org/10.1016/j.jim.2016.01.015.

Aly, A.S.I., Vaughan, A.M., Kappe, S.H.I., 2009. Malaria parasite development in the mosquito and infection of the mammalian host. *Annu Rev Microbiol.* 63, 195–221. doi:10.1146/annurev.micro.091208.073403.

Baldini, F., Gabrieli, P., South, A., Valim, C., Mancini, F., Catteruccia, F., 2013. The interaction between a sexually transferred steroid hormone and a female protein regulates oogenesis in the malaria mosquito Anopheles gambiae. *PLoS Biol.* 11, e1001695. doi:10.1371/journal.pbio.1001695.

Beaty, B.J., Marquardt, W.C., 1996. The biology of disease vectors. University Press of Colorado, Niwot, CO, 1st edition.

Becker, K., Jährling, N., Saghafi, S., Weiler, R., Dodt, H.U., 2012. Chemical Clearing and Dehydration of GFP Expressing Mouse Brains. *PLoS One.* 7(3): e33916. doi: 10.1371/journal.pone.0033916.

Burda, P.C., Roelli, M.A., Schaffner, M., Khan, S.M., Janse, C.J., Heussler, V.T., 2015. A Plasmodium phospholipase is involved in disruption of the liver stage parasitophorous vacuole membrane. *PLoS Pathog.* 11(3): e1004760. doi: 10.1371/journal.ppat.1004760.

CDC, 2014. CDC Division of Vector-Borne Diseases [WWW Document]. URL http://www.cdc.gov/ncezid/dvbd/about.html (accessed 23.03.20).

Choumet, V., Carmi-Leroy, A., Laurent, C., Lenormand, P., Rousselle, J.-C., Namane, A., Roth, C., Brey, P.T., 2007. The salivary glands and saliva of Anopheles gambiae as an essential step in the Plasmodium life cycle: A global proteomic study. *Proteomics.* 7(18): 3384–3394. doi:10.1002/pmic.200700334.

Chung, K., Wallace, J., Kim, S.Y., Kalyanasundaram, S., Andalman, A.S., Davidson, T.J., Mirzabekov, J.J., Zalocusky, K.A., Mattis, J., Denisin, A.K., Pak, S., Bernstein, H., Ramakrishnan, C., Grosenick, L., Gradinaru, V., Deisseroth, K., 2013. Structural and molecular interrogation of intact biological systems. *Nature.* 497(7449): 332–337. doi: 10.1038/nature12107.

De Niz, M., Spadin, F., Marti, M., Stein, J. V, Frenz, M., Frischknecht, F., 2019a. Toolbox for in vivo imaging of host–parasite interactions at multiple scales. *Trends Parasitol.* 35(3): 193–212. doi:https://doi.org/10.1016/j.pt.2019.01.002.

De Niz, M., Meehan, G.R., Brancucci, N.M.B., Marti, M., Rotureau, B., Figueiredo, L.M., Frischknecht, F., 2019b. Intravital imaging of host-parasite interactions in skin and adipose tissues. *Cell Microbiol.* 21(5): e13024. doi: 10.1111/cmi.13023.

De Niz, M., Nacer, A., Frischknecht, F., 2019c. Intravital microscopy: Imaging host-parasite interactions in the brain. *Cell Microbiol.* 21(5): e13024. doi:10.1111/cmi.13024.

De Niz, M., Meehan, G.R., Tavares, J., 2019d. Intravital microscopy: Imaging host-parasite interactions in lymphoid organs. *Cell Microbiol.* 21(12):e13117. doi:10.1111/cmi.13117.

De Niz, M., Carvalho, T., Penha-Goncalves, C., Agop-Nersesian, C., 2020. Intravital imaging or host-parasite interactions in organs of the thoracic and abdomino-pelvic cavities. *Cell Microbiol.* 9:e13201. doi:10/1111/cmi.13201.

Dent, J.A., Polson, A.G., Klymkowsky, M.W., 1989. A whole-mount immunocytochemical analysis of the expression of the intermediate filament protein vimentin in Xenopus. *Development.* 105(1), 61-74.

Dodt, H.U., Leischner, U., Schierloh, A., Jahrling, N., Mauch, C.P., Deininger, K., Deussing, J.M., Eder, M., Zieglgansberger, W., Becker, K., 2007. Ultramicroscopy: three-dimensional visualization of neuronal networks in the whole mouse brain. *Nat Methods.* 4(4): 331–336. doi: 10.1038/nmeth1036.

Eldridge, B.F., Edman, J.D., 2000. Medical Entomology. Springer Netherlands: Kulwer Academic Publishers.

Ertürk, A., Becker, K., Jährling, N., Mauch, C.P., Hojer, C.D., Egen, J.G., Hellal, F., Bradke, F., Sheng, M., Dodt, H.U., 2012. Three-dimensional imaging of solvent-cleared organs using 3DISCO. *Nat Protoc.* 7(11): 1983–1995. doi: 10.1038/nprot.2012.119.

Frischknecht, F., Baldacci, P., Martin, B., Zimmer, C., Thiberge, S., Olivo-Marin, J.C., Shorte, S.L., Menard, R., 2004, Imaging movement of malaria parasites during transmission by Anopheles mosquitoes, *Cell Microbiol.* 6 (7), 687-694. doi:10.1111/j.1462-5822.2004.00395.x

Frischknecht, F., Martin, B., Thiery, I., Bourgouin, C., Menard, R., 2006. Using green fluorescent malaria parasites to screen for permissive vector mosquitoes. *Malar J.* 5:23, 1–8. doi:10.1186/1475-2875-5-23

Genina, E.A., Bashkatov, A.N., Tuchin, V.V., 2010. Tissue optical immersion clearing. *Expert Rev Med Devices.* 7(6), 825–842. doi:10.1586/erd.10.50

Gerger, A., Koller, S., Kern, T., Massone, C., Steiger, K., Richtig, E., Kerl, H., Smolle, J., 2005. Diagnostic Applicability of In Vivo Confocal Laser Scanning Microscopy in Melanocytic Skin Tumors. *J Invest Dermatol.* 124 (3): 493–498. doi:http://dx.doi.org/10.1111/j.0022-202X.2004.23569.x

Gualda, E.J., Vale, T., Almada, P., Feijó, J.A., Martins, G.G., Moreno, N., 2013. OpenSpinMicroscopy: an open-source integrated microscopy platform. *Nat Methods.* 10 (7): 599-600. doi: 10.1038/nmeth.2508.

Ha, Y.R., Lee, S.C., Seo, S.J., Ryu, J., Lee, D.K., Lee, S.J., 2015. Comparison of the functional features of the pump organs of Anopheles sinensis and Aedes togoi. *Sci Rep.* 5, 15148. doi: 10.1038/srep15148.

Hama, H., Hioki, H., Namiki, K., Hoshida, T., Kurokawa, H., Ishidate, F., Kaneko, T., Akagi, T., Saito, T., Saido, T., Miyawaki, A., 2015. ScaleS: an optical clearing palette for biological imaging. *Nat Neurosci.* 18(10): 1518–1529. doi: 10.1038/nn.4107.

Hama, H., Kurokawa, H., Kawano, H., Ando, R., Shimogori, T., Noda, H., Fukami, K., Sakaue-Sawano, A., Miyawaki, A., 2011. Scale: a chemical approach for fluorescence imaging and reconstruction of transparent mouse brain. *Nat Neurosci.* 14 (11), 1481–1488. doi: 10.1038/nn.2928.

Huisken, J., Swoger, J., Del Bene, F., Wittbrodt, J., Stelzer, E.H.K., 2004. Optical sectioning deep inside live embryos by selective plane illumination microscopy. *Science.* 305(5686), 1007–1009. doi:10.1126/science.1100035

Jährling, N., Becker, K., Schönbauer, C., Schnorrer, F., Dodt, H.-U., 2010. Three-dimensional reconstruction and segmentation of intact Drosophila by ultramicroscopy. *Front Syst Neurosci.* 4: 1. doi:10.3389/neuro.06.001.2010

Kak, A.C., Slaney, M., 1988. Principles of Computerized Tomographic Imaging. IEEE Press.

Ke, M.T., Fujimoto, S., Imai, T., 2013. SeeDB: a simple and morphology-preserving optical clearing agent for neuronal circuit reconstruction. *Nat Neurosci.* 16 (8): 1154–1161. doi:10.1038/nn.3447.

Kettle, D.S., 1995. Medical and veterinary entomology. University Press, Cambridge.

Krenn, H.W., Aspöck, H., 2012. Form, function and evolution of the mouthparts of blood-feeding Arthropoda. *Arthropod Struct Dev.* 41(2): 101–118. doi:http://dx.doi.org/10.1016/j.asd.2011.12.001

Lefevre, T., Thomas, F., Schwartz, A., Levashina, E., Blandin, S., Brizard, J.-P., Le Bourligu, L., Demettre, E., Renaud, F., Biron, D.G., 2007. Malaria Plasmodium agent induces alteration in the head proteome of their Anopheles mosquito host. *Proteomics.* 7(11): 1908–1915. doi:10.1002/pmic.200601021

Lehane, M.J., 1991. Biology of Blood-sucking insects. Harper Collins Academic.

Liu, A., Xiao, W., Li, R., Chen, L., Comparison of optical projection tomography and light-sheet fluorescence microscopy, *J Microsc.* 275(1): 3-10. doi: 10.1111/jml.12796.

Macdonald, G., 1956. Theory of the eradication of malaria. Bull. World Health Organ. 15, 369–387.

Maekawa, E., Aonuma, H., Nelson, B., Yoshimura, A., Tokunaga, F., Fukumoto, S., Kanuka, H., 2011. The role of proboscis of the malaria vector mosquito Anopheles stephensi in host-seeking behavior. *Parasit Vectors.* 4:10. doi:10.1186/1756-3305-4-10

Mayer, J., Robert-Moreno, A., Danuser, R., Stein, J.V., Sharpe J., Swoger, J., 2014. OPTiSPIM: integrating optical projection tomography in light sheet microscopy extends specimen characterization to nonfluorescent contrasts. *Opt Lett.* 39(4): 1053–1056. doi: 10.1364/OL.39.001053.

McGurk, L., Morrison, H., Keegan, L.P., Sharpe, J., O'Connell, M.A., 2007. Three-Dimensional Imaging of Drosophila melanogaster. *PLoS One.* 2, e834. doi:10.1371/journal.pone.0000834

Mitchell, S.N., Kakani, E.G., South, A., Howell, P.I., Waterhouse, R.M., Catteruccia, F., 2015. Mosquito Biology. Evolution of sexual traits influencing vectorial capacity in anopheline mosquitoes. *Science.* 347(6225): 985–988. doi:10.1126/science.1259435

Mori, T., Hirai, M., Mita, T., 2019. See-through observation of malaria parasite behaviors in the mosquito vector. *Sci Rep.* 9, 1768. doi:10.1038/s41598-019-38529-3

Ntziachristos, V., 2010. Going deeper than microscopy: the optical imaging frontier in biology. *Nat Meth.* 7, 603–614. doi:10.1038/nmeth.1483.

Pampaloni, F., Reynaud, E.G., Stelzer, E.H.K., 2007. The third dimension bridges the gap between cell culture and live tissue. *Nat Rev Mol Cell Biol.* 8(10): 839–845. doi:10.1038/nrm2236.

Pitrone, P.G., Schindelin, J., Stuyvenberg, L., Preibisch, S., Weber, M., Eliceiri, K.W., Huisken, J., Tomancak, P., 2013. OpenSPIM: an open-access light-sheet microscopy platform. *Nat Meth.* 10(7): 598–599. doi:10.1038/nmeth.2507.

Poguzhelskaya, E., Artamonov, D., Bolshakova, A., Vlasova, O., Bezprozvanny, I., 2014. Simplified method to perform CLARITY imaging. *Mol Neurodegener.* 9:19. doi:10.1186/1750-1326-9-19

Prado, M., Eickel, N., De Niz, M., Heitmann, A., Agop-Nersesian, C., Wacker, R., Schmuckli-Maurer, J., Caldelari, R., Janse, C.J., Khan, S.M., May, J., Meyer, C.G., Heussler, V.T., 2015. Long-term live imaging reveals cytosolic immune responses of host hepatocytes against Plasmodium infection and parasite escape mechanisms. *Autophagy.* 11(9): 1561–1579. doi:10.1080/15548627.2015.1067361

Reynaud E.G., Peychl, J., Huisken, J., Tomancak, P., 2015. Guide to light-sheet microscopy for adventurous biologists. *Nat Methods.* 12: 30-34. doi:10.1038/nmeth.3222

Ribeiro, J.M., Rossignol, P.A., Spielman, A., 1984. Role of mosquito saliva in blood vessel location. *J Exp Biol.* 108, 1-7.

Rono, M.K., Whitten, M.M.A., Oulad-Abdelghani, M., Levashina, E.A., Marois, E., 2010. The major yolk protein vitellogenin interferes with the anti-Plasmodium response in the malaria mosquito Anopheles gambiae. *PLoS Biol.* 8(7): e1000434. doi: 10.1371/journal.pbio.1000434

Rossignol, P.A., Ribeiro, J.M.C., Spielman, A., 1984. Increased Intradermal Probing Time in Sporozoite-Infected Mosquitoes. *Am J Trop Med Hyg.* 33(1): 17–20. doi:10.4269/ajtmh.1984.33.17

Sharpe, J., Ahlgren, U., Perry, P., Hill, B., Ross, A., Hecksher-Sørensen, J., Baldock, R., Davidson, D., 2002. Optical Projection Tomography as a Tool for 3D Microscopy and Gene Expression Studies. *Science.* 296 (5567): 541-545. doi:10.1126/science.1068206.

Silvie, O., Mota, M.M., Matuschewski, K., Prudêncio, M., 2008. Interactions of the malaria parasite and its mammalian host. *Curr Opin Microbiol.* 11 (4): 352–359. doi:http://dx.doi.org/10.1016/j.mib.2008.06.005

Smith, D.L., Battle, K.E., Hay, S.I., Barker, C.M., Scott, T.W., McKenzie, F.E., 2012. Ross, Macdonald, and a Theory for the Dynamics and Control of Mosquito-Transmitted Pathogens. *PLoS Pathog.* 8 (4): 1–13. doi:10.1371/journal.ppat.1002588

Susaki, E.A., Tainaka, K., Perrin, D., Kishino, F., Tawara, T., Watanabe, T.M., Yokoyama, C., Onoe, H., Eguchi, M., Yamaguchi, S., Abe, T., Kiyonari, H., Shimizu, Y., Miyawaki, A., Yokota, H., Ueda, H.R., 2016. Whole-brain imaging with single-cell resolution using chemical cocktails and computational analysis. *Cell.* 157 (3): 726–739. doi:10.1016/j.cell.2014.03.042

Takken, W., Knols, B.G.J., 1999. Odor-mediated behavior of Afrotropical malaria mosquitoes. *Annu Rev Entomol.* 44, 131–157. doi:10.1146/annurev.ento.44.1.131

Vallejo Ramirez, P.P., Zammit, J., Vanderpoorten, O., Riche, F., Blé, F.-X., Zhou, X.H., Spiridon, B., Valentine, C., Spasov, S.P., Oluwasanya, P.W., Goodfellow, G., Fantham, M.J., Siddiqui, O., Alimagham, F., Robbins, M., Stretton, A., Simatos, D., Hadeler, O., Rees, E.J., Ströhl, F., Laine, R.F., Kaminski, C.F., 2019. OptiJ: Open-source optical projection tomography of large organ samples. *Sci Rep.* 9(1):15693. doi:10.1038/s41598-019-52065-0

Whitten, M.M.A., Shiao, S.H., Levashina, E.A., 2006. Mosquito midguts and malaria: cell biology, compartmentalization and immunology. *Parasite Immunol.* 28(4): 121–130. doi:10.1111/j.1365-3024.2006.00804.x

WHO, 2015. World Malaria Report.

Won Jung, J., Baeck, S.J., Perumalsamy, H., Hansson, B.S., Ahn, Y.J., Kwon, H.W., 2015. A novel olfactory pathway is essential for fast and efficient blood-feeding in mosquitoes. *Sci Rep.* 5, 13444. doi: 10.1038/srep13444.

Figure S1

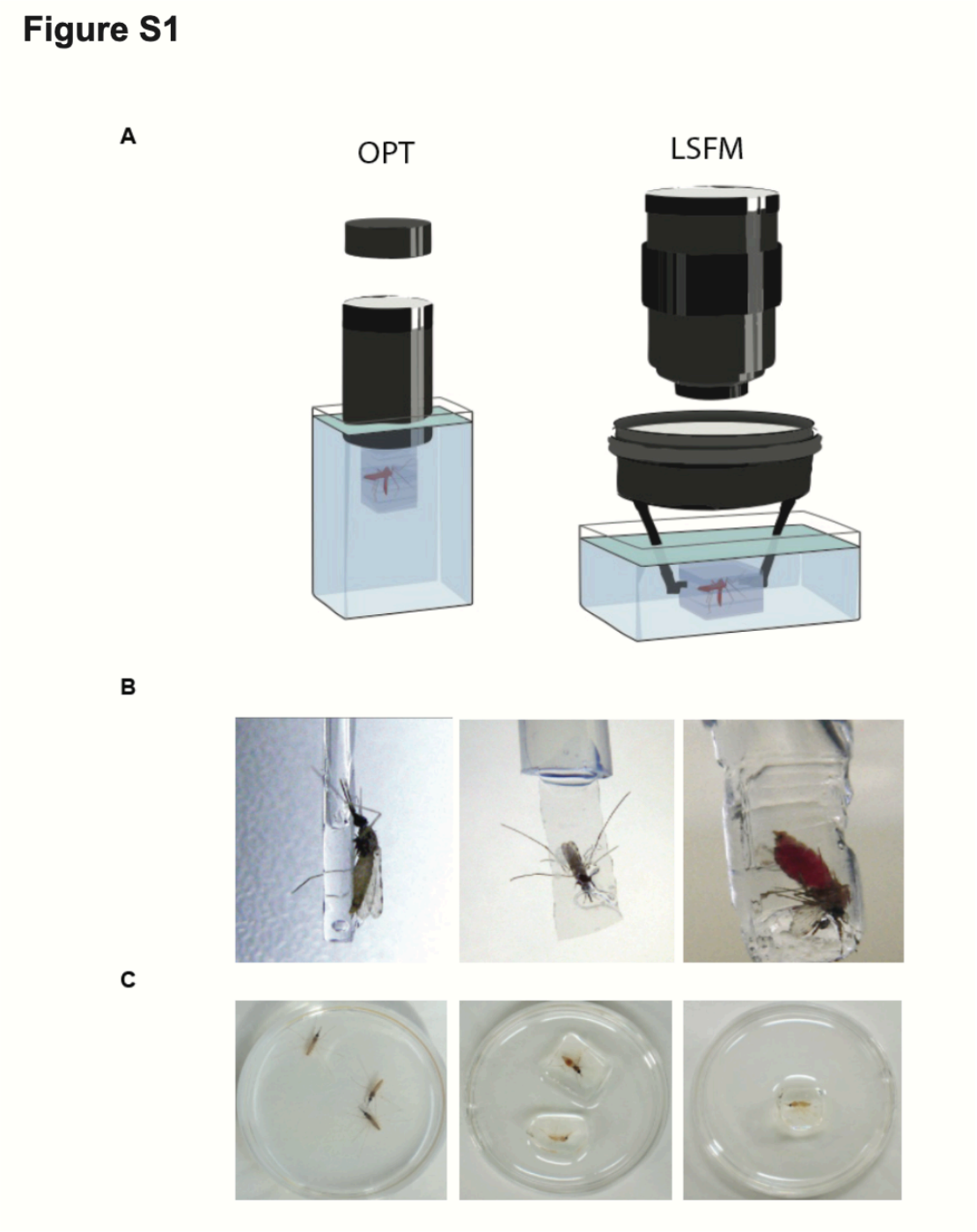

Figure S1. Mosquito mounting and embedding. A) OPT imaging requires embedding the mosquito in low-melting temperature ultrapure agarose gel, and mounting it onto a metallic cylinder that is attached to a rotating stage via a magnet. The embedded attached mosquito is then lowered into a chamber containing index-matching liquid, such as Murray's clear medium. The setup for Ultramicroscopy imaging involves embedding the mosquito in low-melting temperature ultrapure agarose gel, and mounting it on a lower ring of the customized holder. Both the holder and the embedded mosquito are submerged into a chamber containing index-matching liquid. **B)** Methods for mounting mosquitoes to enable imaging and rotation. **C)** Petri dishes showing (1) fixed mosquitoes prior to optical clearance and embedding and (2) optically cleared mosquitoes embedded in ultrapure low-melting temperature agarose.

Figure S2

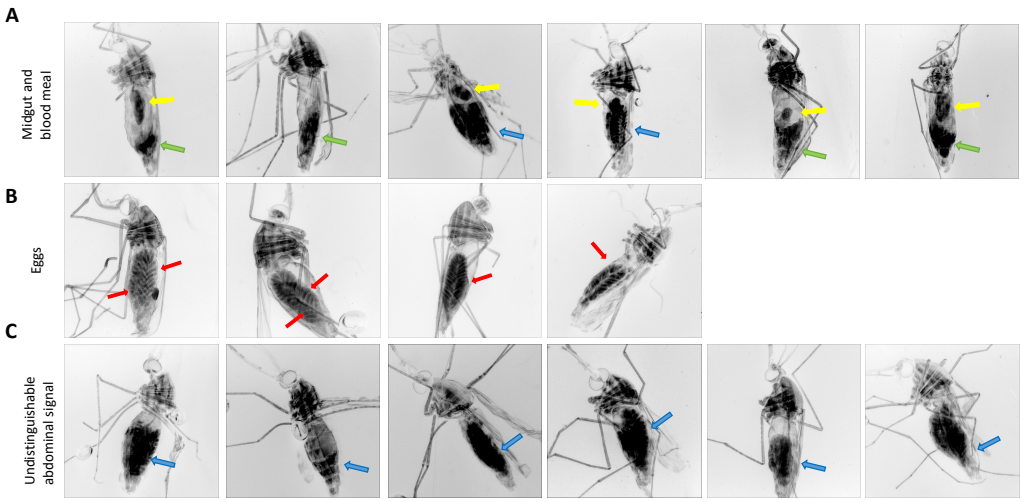

Figure S2. Detected fluorescence and autofluorescence signals in undissected mosquitoes. Given the very successful clearance obtained with BABB, fluorescence quenching occurs. We show in this panel various possible outcomes of clearance using BABB, including **A)** a mixture of detectable fluorescence in the midgut (yellow arrows), clear autofluorescence arising lower in the body (green arrows) and autofluorescence arising from eggs (blue arrows); **B)** clear autofluorescence arising from the eggs, but no other detectable signal in the abdomen; **C)** indistinguishable abdominal signal, without the possibility of distinguishing the bloodmeal from the eggs and potential parasites in the midgut.

Figure S3

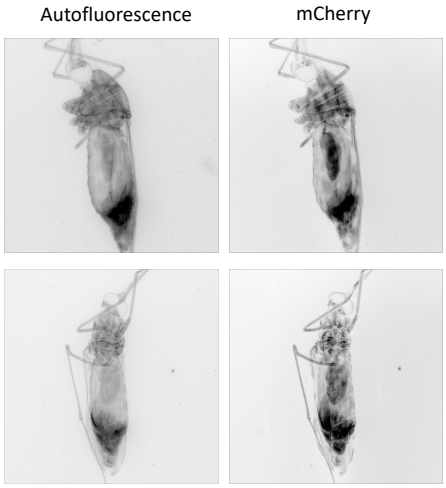

Figure S3. Specific fluorescence. Examples obtained from Figure S2, showing separate autofluorescence an mCherry signal, demonstrating preservation of mCherry.

Movie 1. 3D visualization of an optically cleared *Anopheles stephensi* female mosquito, imaged by optical projection tomography.

Movie 2. 3D visualization of an optically cleared *Anopheles stephensi* mosquito midgut, imaged by LSFM. Fluorescent bodies correspond to *Plasmodium* oocysts.

Table 1. Comparison of clearing methods for mosquito cuticle

Method	**Principle**	**Time to achieve tissue transparency**	**Preservation of fluorescence signal**	**Preservation of tissue morphology**
3DISCO	Organic solvent	20-30 days (++)	+	Unaltered
BABB (Murray's clear)	Organic solvent	5-10 days (+++)	+	Slight dehydration
ScaleS	Water-based	Partial clearance at 30 days (+/-)	+++	Unaltered
SeeDB	Water-based	Partial clearance at 30 days (+/-)	+++	Unaltered

Table 2. Comparison of OPT/LSFM with other microscopy procedures

Method	Principle	Advantage	Disadvantage
Widefield microscopy	Light passes through the sample, maximizing illumination	Simple to perform. Fluorescence detection possible. Live imaging possible.	Does not allow acquisition of detailed parasite development or localization. For this, it would require physical sectioning.
Confocal microscopy	Increases optical resolution by means of a pinhole that blocks out of focus light.	Higher optical resolution possible. Visualization of specific structures and their interactions possible. Live imaging possible.	Requires optical sectioning. 3D reconstruction of a full sample is time consuming. If sample uncleared, scattering is problematic.
Two photon microscopy	Two low energy photons cooperate to cause a higher-energy electronic transition in a fluorescent molecule.	Penetration of up to 1mm of depth, and minimization of phototoxicity. Live imaging possible.	Requires optical sectioning. 3D reconstruction of a full sample is time consuming. If sample uncleared, scattering is problematic.
Electron microscopy	Uses beam of accelerated electrons as a source of illumination.	Very high resolution achievable. Information on details of structures, tissues, cells, organelles and sub-organellar structures easy to obtain.	Sample cannot be live. Method for sample preparation is complex and time consuming. Full mosquito reconstruction would be very time consuming.
OPT	Form of tomography involving optical microscopy that allows full 3D sample reconstruction.	Fluorescence based method. Allows detailed visualization and 3D reconstruction. Does not require physical sectioning of the sample.	Requires optimization of tissue clearance and fluorescence preservation. At the moment cannot be used in live samples.
LSFM	Sample scanning with a plane of light.	Fluorescence based method. High optical resolution and high acquisition speed. Allows detailed visualization and 3D reconstruction. Does not require physical sectioning of the sample.	Requires optimization of tissue clearance and fluorescence preservation. At the moment cannot be used in live samples.